AFRL-SR-AR-TR-09-0071

REPORT DOCUMENTATION PAGE

1. REPORT DATE *(DD-MM-YYYY)*	2. REPORT TYPE	3. DATES COVERED *(From - To)*
02/02/2009	Final Performance Report	12/01/2005 to 11/30/2008

4. TITLE AND SUBTITLE
In-Fiber Magneto-Optic Devices Based on Ultrahigh Verdet Constant Organic Materials and Holey Fibers

5a. CONTRACT NUMBER

5b. GRANT NUMBER
FA9550-06-1-0039

5c. PROGRAM ELEMENT NUMBER

6. AUTHOR(S)
Nasser Peyghambarian
Robert A. Norwood
Andre Persoons

5d. PROJECT NUMBER

5e. TASK NUMBER

5f. WORK UNIT NUMBER

7. PERFORMING ORGANIZATION NAME(S) AND ADDRESS(ES)

Arizona Board of Regents,
University of Arizona
888 N. Euclid Ave, Room 510
Tucson, AZ 85721-0158

8. PERFORMING ORGANIZATION REPORT NUMBER

9. SPONSORING / MONITORING AGENCY NAME(S) AND ADDRESS(ES)

USAF, AFRL/NA
AF Office of Scientific Research
875 N. Randolph St., Room 3112
Arlington, VA 22203

Office of Naval Research (ONRRO)
San Diego Regional Office
4520 Executive Dr., Suite 300
San Diego, CA 92121-3019

10. SPONSOR/MONITOR'S ACRONYM(S)

11. SPONSOR/MONITOR'S REPORT NUMBER(S)

12. DISTRIBUTION / AVAILABILITY STATEMENT
Distribution unlimited.

13. SUPPLEMENTARY NOTES

14. ABSTRACT A high sensitivity Verdet constant measurement system was developed that obtained Verdet constants for commercially available standards in excellent agreement with the literature. We have observed Verdet constants of approximately 100,000 degrees/T-m in regioregular polythiophenes and shown that the regioregularity and processing conditions critically effect their properties. New magnetite nanoparticle/acrylate polymer core/shell nanocomposites with exceptional transparency across the visible/IR have been developed. These composites exhibit Verdet constants > 100,000 degrees/T-m in pristine films and > 1,000,000 degrees/T-m in magnetic field poled films at a few weight percent nanoparticle loading. Our unique polymer synthesis allows us to tune the refractive index of the final composite. We have demonstrated waveguide Faraday rotation (2 degrees) using a magnetic field poled nanocomposite as the cladding for a sol-gel waveguide core, and further optimization of optical properties, poling, magnetic field delivery and nanoparticle loading should give the rotation required for an isolator. A garnet-based magnetic field sensor working at about 100 pT has also been demonstrated. KU Leuven provided regioregular polythiophenes and magnetite nanoparticles for our studies.

15. SUBJECT TERMS

16. SECURITY CLASSIFICATION OF:			17. LIMITATION OF ABSTRACT	18. NUMBER OF PAGES	19a. NAME OF RESPONSIBLE PERSON
a. REPORT	b. ABSTRACT	c. THIS PAGE			Nasser Peyghambarian
					19b. TELEPHONE NUMBER *(include area code)* (520) 621-4649

FINAL REPORT

"In-fiber Magneto-optic Devices Based on Ultrahigh Verdet Constant Organic Materials and Holey Fibers"

College of Optical Sciences University of Arizona
1630 E. University Blvd
Tucson, AZ 85721-0094

Grant number # FA9550-06-1-0039

Nasser Peyghambarian, Robert A. Norwood, André Persoons

In-fiber Magneto-optic Devices Based on Ultrahigh Verdet Constant Organic Materials and Holey Fibers

A high precision magneto-optic rotation measurement setup that can measure ultra-small Faraday rotation has been developed. Efficient noise cancellation methods have been employed in the demonstration of weak (~ 100 pT) magnetic field sensing at very low frequency (20 – 1000 Hz). Magnetic and magneto-optic (MO) properties of polythiophene derivatives have been investigated in order to elucidate a structure-property relationship.

- ***Faraday rotation measurement setup:*** A setup to measure Faraday rotation of thin polymer films was designed and implemented, taking advantage of custom-made air-core solenoids, efficient noise cancellation in an auto-balanced detection system and lock-in amplifier detection techniques. A selection of commercially available MO materials has been used to construct low frequency magnetic field sensors working at various wavelengths. An all-fiber magnetic field sensors has been constructed using similar noise cancellation and detection protocols and a noise equivalent magnetic field sensitivity of ~ 100 pT/ $\sqrt{Hz}$ has been demonstrated.

- ***Magneto-optic properties of magnetite – PMMA composite***: Developed acrylate polymer/magnetite nanoparticle composites exhibiting Verdet constants > 10^{6}°/T-m in poled films; these nanocomposites are the first core-shell type MO material developed based on nanoparticles and possess high optical transparency across the visible and IR region.

- ***Developed fiber-based magnetic field sensor***: A magnetic field sensor working within the range of 100 to 400 *pico tesla* using a garnet-based slab waveguide has been demonstrated.

- ***Demonstration of Faraday rotation in waveguides***: Initial demonstration of waveguide Faraday rotation (2°) using a poled acrylate polymer/magnetite nanoparticle composite as the cladding material;

- ***Magneto-optic properties of polythiophene derivatives:*** A pool of different polythiophene-based polymers with varying molecular structure and regioregularity has been studied. The Faraday rotation measured on the thin, spun-coat films of these polymers was found to be dependent on many factors, mainly on the regioregularity, processing conditions and molecular structure. Verdet constants on the order of 10^{5}°/T-m or more were measured in this class of polymers.

- ***Magnetic properties of polythiophene derivatives:*** We have shown that regioregular poly(3-dodecyl)thiophene is ferromagnetic at low temperature (7 °K) and behaves as a blocked superparamagnetic system at higher temperatures. Notably, this is the only observed organic polymer magnetic system based upon a highly correlated electronic spin system.

Abstract

A high sensitivity Verdet constant measurement system was developed that obtained Verdet constants for commercially available standard materials in excellent agreement with the literature. We have observed Verdet constants on the order of 10^5°/T-m in regioregular polythiophenes and demonstrated that the regioregularity and processing conditions critically effect their magneto-optic (MO) properties. An array of new magnetite nanoparticle/acrylate polymer core/shell nanocomposites with exceptional transparency across the visible and IR region have been developed. These composites exhibit Verdet constants > 10^5°/T-m in pristine films and > 10^6 °/T-m in magnetic field poled films at a few weight percent loading of Fe_3O_4 nanoparticles. Our unique two-step bottom-up synthesis of these polymers allows us to tune the refractive index of the final composite, a critical requirement for effective fabrication of waveguide devices. We have demonstrated waveguide Faraday rotation (~2°) using a magnetic field poled nanocomposite as the cladding material for a sol-gel waveguide core, and further optimization of refractive indices, birefringence, poling, magnetic field delivery and nanoparticle loading are expected to give the 45° rotation required for an isolator. A magnetic field sensor working within the range of 100 to 400 *pico tesla* using a garnet-based slab waveguide has also been demonstrated. KU Leuven provided regioregular polythiophenes and some magnetite nanoparticles for our studies and collaborators at WPAFB have extended their synthetic capabilities for developing magnetic ionic liquids, first developed and screened at the University of Arizona under this project.

1. SUMMARY

- Developed a high sensitivity Verdet constant measurement system using a high common mode noise rejection ratio that is capable of measuring Faraday rotation on the order of 10^{-6} °;
- Observed a large Faraday rotation in regioregular polythiophene with a maximum Verdet constant of 1.4×10^{5}°/T-m;
- Performed detailed magnetization studies and demonstration of the ferromagnetic phase in regioregular poly(3-dodecyl)thiophene;
- Developed acrylate polymer/magnetite nanoparticle composites exhibiting Verdet constants $> 10^{6}$°/T-m in poled films;
- Developed a magnetic field sensor with magnetic field sensitivity of 300 pT/√Hz based on commercially available garnet material;
- Designed a polarization independent waveguide based optical isolator and demonstrated operation of all of the passive elements of the isolator including a polarization splitter, a waveguide waveplate giving 45° reciprocal rotation, and a polarization coupler, taking advantage of a new polymer (PCDY50) with very large photoinduced birefringence ($\Delta n \sim 0.2$);
- Initial demonstration of waveguide Faraday rotation (~2°) using a poled acrylate polymer/magnetite nanoparticle composite as the cladding material;

2. OBJECTIVES

The main objective of this work is to create in-fiber or waveguide optical isolators and other magneto-optic devices useful for various DOD, communications, sensing, and medical applications working in the visible as well as at 980 nm, 1310 nm and 1550 nm and based on the ultrahigh Verdet constants (~10^5 degree$T^{-1}m^{-1}$) of substituted polythiophene material recently developed by us. The primary objectives of this project are as follows:

- To understand and further explore the origins of the very large magneto-optic (MO) effects that we have recently observed in doped and undoped polythiophene compounds, with the goal of elucidating key structure-property relationships and using knowledge of these relationships to create optimized materials that have high Verdet constants, low optical loss, excellent thermal stability, resistance to photo-induced damage, and good processability;
- To create in-fiber optical isolators and other magneto-optic devices based upon the parallel development of ultrahigh Verdet constant materials and polymer based waveguides.

The key steps required to achieve these objectives are as follows:

- Establish a high precision system to measure Verdet constants of thin organic films.
- Measure 1-2 μm range Verdet constants for solution/melt processed polythiophene materials.
- Evaluate additional candidate organic MO materials and investigate structure-property relationships to identify the underlying mechanism behind the MO activity in these materials.
- Evaluate candidate materials based on magnetic nanoparticles/polymer nanocomposites and commercially available Garnet materials.
- Optimize polymer MO materials to identify a suitable candidate for isolators.
- Develop micro-structured fiber and waveguide structures suitable for incorporation of polymer MO materials.
- Fabricate and characterize fiber and waveguide based devices.

3. STATUS OF EFFORT

The primary objective of this program is to develop a compact, low cost, polymer-based in-fiber /waveguide optical isolator that can be readily integrated with a large range of photonic integrated circuit (PIC) technologies including semiconductors, glass and polymers operating between 0.83μm and 1.55μm wavelengths. The University of Arizona has successfully collaborated with the Prof. Andre Persoons group at the Catholic University of Leuven, Belgium to exploit the extensive research they have carried out in the field of polymers with extraordinarily high MO activity. At the outset of this program, conjugated polymers were available with up to four orders of magnitude higher Verdet constants than those of previously known commercial MO materials, and while these polythiophenes continue to be of interest, research at the University of Arizona showed that new polymer nanoparticle composite materials would be cheaper and a viable alternative to polythiophenes. Furthermore, the nanocomposite materials provide the ability to directly engineer the optical and MO properties of the material; the recent development of poling techniques results in Verdet constants in excess of those available from the polythiophenes (> 1 × $10^{6°}$/T-m). To fully exploit these materials developments, necessary elements required to implement a polarization independent optical isolator have been designed and developed. Faraday rotation of ~ 2 ° has been demonstrated in

magnetite polymer nanocomposite based waveguides and work is underway to increase the rotation to the 45 ° required for an isolator. In the course of this work, extensive investigation has been carried out to elucidate structure-property relationships with the class of substituted polythiophenes.

4. ACCOMPLISHMENTS/NEW FINDINGS

A high sensitivity Verdet constant measurement system was developed that obtained Verdet constants for commercially available standard materials in excellent agreement with the literature. Verdet constants on the order of 10^5°/T-m in regioregular polythiophenes have been measured and demonstrated that the regioregularity and processing conditions critically affect their magneto-optic MO properties. An array of new magnetite nanoparticle/acrylate polymer core/shell nanocomposites with exceptional transparency across the visible and IR region have been developed. These composites exhibit Verdet constants > 10^5°/T-m in pristine films and > 10^6 °/T-m in magnetic field poled films at a few weight percent loading of Fe_3O_4 nanoparticles. Our unique two-step bottom-up synthesis of these polymers allows tuning of the refractive index of the final composite, a critical requirement for effective fabrication of waveguide devices. Waveguide Faraday rotation (~ 2°) has been demonstrated using a magnetic field poled nanocomposite as the cladding material for a sol-gel waveguide core, and further optimization of refractive indices, birefringence, poling, magnetic field delivery and nanoparticle loading are expected to give the 45° rotation required for an isolator. A magnetic field sensor working within the range of 100 to 400 *pico tesla* using a garnet-based slab waveguide has also been demonstrated. KU Leuven provided regioregular polythiophenes and some magnetite nanoparticles for our studies and collaborators at WPAFB have extended their synthetic capabilities for developing magnetic ionic liquids, first developed and screened at the University of Arizona under this project.

4.1. Measurement Setup and Faraday rotation studies on polythiophene derivatives

4.1.1 Introduction.

Faraday rotation[1] is the rotation of the plane of polarization of linearly polarized light due to magnetic field induced circular birefringence of a material. In a non-absorbing or weakly absorbing medium a linearly polarized monochromatic light beam passing through the material along the direction of the applied magnetic field experiences circular birefringence, resulting in rotation of the plane of polarization. The angle of rotation θ is expressed as $\theta = VBL = \pi \frac{\Delta n}{\lambda} L$ where Δn is the magnitude of circular birefringence (the difference between the refractive indices for left and right circularly polarized light in the medium), λ is the wavelength of light, B is the magnetic flux density applied to the material parallel to the propagation direction of light and L is the length of the medium (see Figure 1). The constant V, the Verdet constant (generally expressed in degree/Tesla-meter)

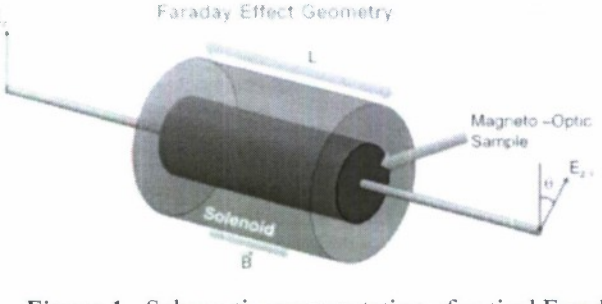

Figure 1. Schematic representation of optical Faraday effect geometry.

is a materials property and a quantitative measure of the Faraday rotation ability of the material. The Verdet constant is strongly wavelength dependent, decreasing dramatically away from resonance and in the case of a paramagnetic material V also depends on the frequency of the magnetic field used.[2] The Verdet constant is usually measured by determining the amount of polarization rotation that linearly polarized light experiences when incident on a sample under an AC or DC magnetic field. Faraday active materials are used in high-end applications such as the optical isolator,[3] an important device that protects lasers from unwanted back reflection, highly sensitive magnetic field sensors,[4] and satellite altitude monitors,[5] among others. Faraday rotation measurements have also been used to estimate magnetic susceptibilities and carrier densities[6] in semiconductors where the effective mass of the carrier is known. Generally, Faraday rotation is at its strongest in inorganic substances containing paramagnetic ions or in superparamagnetic and magnetic materials.[7] Unfortunately, these materials are often very expensive and difficult to process, do not allow for miniaturization and hybrid integration, and/or are not suitable for applications at ambient temperatures. Organic or polymeric materials had not been investigated for efficient Faraday rotation until recently. Nevertheless, a significant advantage of organic materials would be their ease of processing, limited weight and the fact that they can be custom designed and synthesized to meet specific device requirements. Recently we have shown that conjugated polythiophenes are very promising materials for Faraday rotation.[8] We have shown that some of the polythiophene derivatives possess exceptionally high Verdet constants, 200 – 300 times larger than those of commercially used MO materials, such as, terbium doped gallium garnet (TGG) crystals or substituted yttrium iron garnets (YIGs).[9] The potential applications of polymeric MO materials include attractive possibilities of more compact and integrable waveguide optical isolators and high performance magnetic field sensors that can be readily inserted onto photonic integrated circuit platforms for both commercial and military applications.[10]

The instrumentation for Faraday rotation measurement (so-called magneto-optic polarimetry) has continued to attract attention over the last few decades largely because of its application as a highly sensitive photonic magnetic field sensor.[4] The sensing of weak to extremely weak magnetic fields of low frequency (~4 to 60 Hz), *i.e.* those associated with the surveillance of military activities such as moving vehicles or underwater moving objects causing magnetic field fluctuations through interactions with the earth's magnetic field has been explored.[11] Ongoing investigations aim to improve the sensitivity enough to measure sub femto-tesla magnetic fields, a requirement for mapping bio-magnetism such as that occurring in the human brain.[12] Potentially, a highly sensitive Faraday rotation measurement system will enable one to measure MO properties of organic materials, possibly at the single molecule level, opening a hitherto uncharted arena for MO materials. Methods to measure Verdet constants of materials using AC[13] or DC[14] magnetic fields involving either simple polarimetric or the more complex interferometric[15] approach in both free space and in-fiber[16] configurations have been reported in literature. An estimated noise equivalent rotation measurement sensitivity of $3\times10^{-6}\ ^{\circ}/\sqrt{Hz}$ has been reported[17] using interferometric techniques and is among the best sensitivities achieved in bench-top applications. In a high power free space common path polarization Sagnac interferometer shot-noise[18] limited rotation sensitivity of $6\times10^{-8}\ ^{\circ}/\sqrt{Hz}$ has been achieved using a post modulation scheme at 12 MHz.[19] Two techniques fairly common to these measurements are balanced phase sensitive detection combined with polarization modulation and heterodyne detection coupled with a post modulation scheme generally operating in the RF regime. However, a bench-top interferometric setup requires the use of higher laser

power over a larger area to attain shot-noise limited sensitivity. There is a desire to improve the traditional but compact bench-top MO polarimeter to attain similar sensitivity.

We report a simplified free space bench top MO polarimeter using a magnetic field modulation technique and various optical and electronic noise cancellation schemes working together. We used this system for Faraday rotation measurements in reflection and transmission as well as by placing a non-magnetic mirror behind any transparent sample in a two-pass configuration. A comprehensive characterization of the setup using commercially available materials and Faraday rotation measurements on thin films of different polythiophene derivatives are reported here.

4.1.2. Instrumentation

Figure 2 shows a schematic of the setup where the optical beam interacts with the sample twice. Due to the nonreciprocal nature of Faraday rotation, such a two pass setup generates twice the rotation for a similar magnetic field and cancels any rotation present that is reciprocal in nature. Inherent anisotropy in crystals or spun coat thin films and possible scattering from free space optics may generate such reciprocal rotation of polarization as a result of circular birefringence. Instead of a large conventional magnet, smaller, low impedance commercially available solenoids are used. Suitably designed heat sinks are attached to the solenoids to efficiently diffuse the heat generated during long hours of operation. The sinusoidal output from the internal oscillator of the lock-in amplifier, SR830, is fed into the home built low-noise amplifier / solenoid driver to create 20 to 400 Gauss of AC flux density. The magnetic fields are calibrated periodically using a Hall probe AC gauss meter. In this experiment a Glan-Thomson polarizer (extinction ratio, ER = 1:500,000) is used to prepare an incident light beam with a polarization of 45° that passes through the sample placed inside the solenoid. Upon interaction with the sample under the influence of the AC magnetic field the plane of polarization of the light oscillates periodically. The output linearly polarized beam gets reflected by the non magnetic mirror and passes through the sample a second time. A near DC low frequency magnetic field modulation does not destroy the coherence between the forward and backward beam and thereby simplifies the setup. A Wollaston prism (ER = 1:500,000) separates the two linearly polarized components of the output which are subsequently detected by two auto-balanced detectors and a dual phase lock-in amplifier (SR 830). The detectors used here are silicon (for 400 – 1000 nm) and InGaAs (1000 – 1600 nm) based Nirvana auto-balanced front end receivers, Model 2007 and 2017 from New Focus. The wavelengths used in these experiments are 532 nm (from a frequency doubled Nd:YAG solid state laser), 632.8 nm (He-Ne gas laser), 670 nm (solid state diode laser), 980 nm,

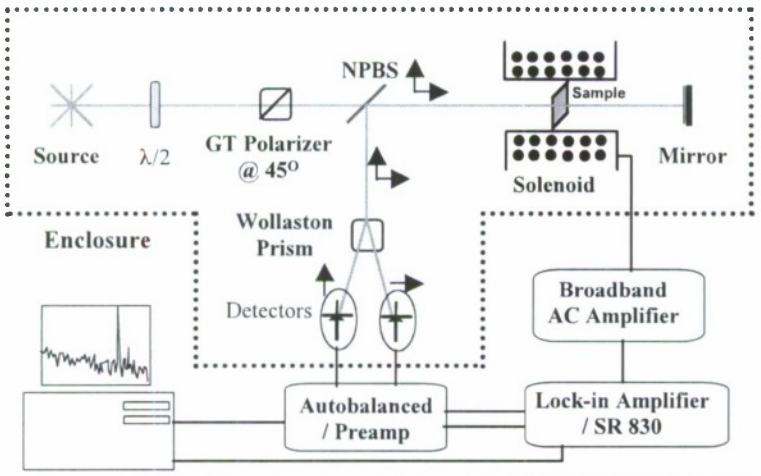

Figure 2: Experimental setup and the polarization states at each location: vertical, in-plane polarization; horizontal, out-of-plane polarization, red solid line is the laser beam and NPBS is a non polarizing beam splitter.

1310 nm and 1550 nm (all DFB diodes). Auto-balanced phase sensitive detection is used to reduce common mode laser noise using the method of comparing one or more signal beams to a reference beam. The measured rotation is generally recovered as a phase change, a ratiometric quantity, unlike the more common traditional polarimetric method, *i.e.*, through a polarizer / rotating analyzer. This causes the setup / detection process to be less affected by the source / detector *1/f* noise down to very low frequency, making it more likely that the ambient noise becomes the largest source of low frequency noise (~ < 1Hz).

The Mueller matrix treatment applied to the optics described above gives us the time varying part of the signal on the Wollaston prism as $\theta = \theta_0 \sin f_m t$ with f_m the frequency of the magnetic field. The Wollaston prism separates the two linearly polarized components and the intensities falling on the two detectors can be described as

$$I_t^h = kI_0 \sin\left(2n\theta_0 \sin f_m t\right) \text{ and } I_t^v = kI_0 \sin\left(\pi/2 - 2n\theta_0 \sin f_m t\right) \text{ respectively} \quad [1].$$

Here n is the number of passes and h and v denotes horizontal and vertical states of polarization, respectively. Applying the Fourier-Bessel transform to **[1]**, using the differential detection method, we get,

$$\theta_0 = \frac{\left|I_{AC}^h(\omega) - I_{AC}^v(\omega)\right|}{2n\left(I_{DC}^h + I_{DC}^v\right)} \; rad \qquad [2]$$

where θ_0 is the Faraday rotation, and I is the measured intensity at the detector for the various polarization and modulation conditions. The sign of the rotation and hence that of the Verdet constant can be determined by careful inspection of the phase estimated by the lock-in amplifier with 180° of phase shift from positive to negative rotation. To examine the performance of the setup in the micro degree range of rotation measurements, we have measured Faraday rotation from a BK7 slab and TGG crystal, each 1 mm thick, under a small magnetic field at 532 nm. The data, presented in Figure 3, gave a Verdet constant value of +356 and -10118 °/T-m for BK7 and TGG respectively, values within 5% of the literature values.[13,20] The data clearly shows the ability of this system to perform micro-degree Faraday rotation measurements; the noise equivalent sensitivity of the setup is dependent on many factors, such as wavelength and optical power of the laser, measurement time and bandwidth, etc.; a detailed discussion

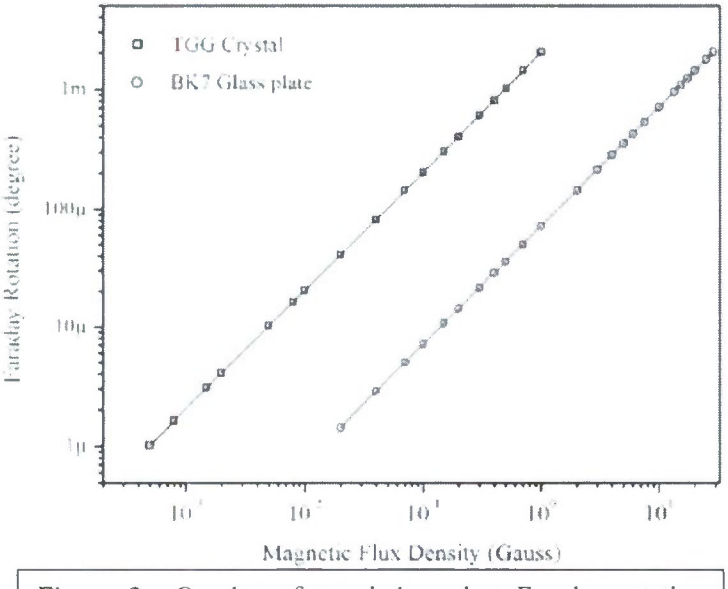

Figure 3. Overlay of two independent Faraday rotation measurements on a TGG crystal and a BK7 glass plate, each of 1 mm thickness, under magnetic fields at 400 Hz. A cw 532nm laser was used with appropriate power adjustments so that the power ratio at the two detectors was 1:2 with a maximum of 1 mW of power at each detector.

of the sensitivity analysis is out of the scope of this report. With a minimum signal to noise ratio of 10, at 532 nm, the setup has a sensitivity of 10^{-6} °/√Hz, when used with at least 2 mW of optical power, sensitivity increasing with optical power. In the absence of any standard MO materials, to evaluate repeatability and performance of the system at various wavelengths, Faraday rotation in a variety of materials, including glass, liquid solvents and crystals was measured and compared with the values available in literature. The comparison, presented in Table 1 shows that the measurements are repeatable within 5% and compare well with the reported values. Efficient noise cancellation, high repeatability, and sensitivity of the setup have been the key factors in our ability to measure Faraday rotation from the ultra-thin films of regioregular alkyl substituted polythiophenes.

Table 1. Measured Verdet constants (°/T-m) of different materials at various wavelengths are listed below. The bracketed values are the standard deviation calculated from several independent measurements. The values noted in bold below the measured value are reported in the literature for the corresponding material. TGG was oriented along the 111 crystallographic plane.

	532 nm	633 nm	670 nm	980 nm	1310 nm	1550 nm
Toluene[21]	+542 (2)	+351(1)	+310 (1)	+71 (1)	+33 (.5)	+19 (.2)
	547	**357**	**315**	**73**	**35**	**29**
p-Xylene[39]	+507 (2)	+329 (2)	+290 (1)	+52 (.5)	+28 (.2)	+10 (.2)
	510	**338**	**306**	**53**	**28**	**14**
BK7[18]	+356 (.5)	+254 (.3)	+233 (.5)	+106 (.6)	+74 (1)	+45 (2)
	367	**270**	**240**	-	-	-
TGG[19]	-10118 (45)	-8128 (22)	-7292 (18)	-3420 (12)	-2274 (20)	-1544 (20)
	-10330	**-8335**	**-7500**	**-3385**	-	-

4.1.3 Materials and Methods

Polymers: Poly(3-hexylthiophene-2,5-diyl) regioregular (RRP3HT), average M_n ~17,500 and poly(3-dodecylthiophene-2,5-diyl) regioregular (RRP3DT), average M_n ~27,000 with regioregularity for the chain (without the head-group) > 99% and their respective regio-random analogues (P3HT and P3DT) were used as procured. TGG crystal, optical quality BK7 slabs and solvents toluene and *p*-xylene were also purchased from different commercial sources and used as is. Absorption spectra of RRP3HT, RRP3DT and P3DT thin films were recorded using a Cary 5G UV-VIS-NIR spectrophotometer. Small angle X-ray diffraction was recorded at ambient temperature using a Scintag XDS 2000 PTS diffractometer. An Innova scanning probe microscope (SPM) from Veeco Systems was used for atomic force microscope (AFM) experiments on the spun coat 1 μm thick RRP3DT films deposited on Si substrates. In a typical Faraday rotation measurement, the film is spun coat from a suitable solvent/solution (filtered through 0.45 μm filter) on a cleaned BK7 glass substrate. BK7 plates are generally cleaned using piranhic acid (1:3 sulphuric acid and hydrogen peroxide mixture) followed by thorough cleaning with water. The spun-coat films are prepared with high speed spinning (up to 3000 rpm) in a Class 100 clean room. After the Faraday rotation measurements are completed, thicknesses of these films are determined using atomic force microscopy (AFM). The films are subsequently removed from the substrate and the Faraday rotation of the bare substrate is measured. By subtracting the rotation of the bare substrate from that of the film, the net rotation of the material is determined.

4.1.4 Results and Discussion

Regioregular (RR) substituted alkyl thiophene derivatives, such as RRP3DT and RRP3HT (Figure 4), in which the hexyl and dodecyl side groups are attached to the third position of the thiophene ring in a head-to-tail stereoregular order, are known to form thin films with nanocrystalline lamellae.[22] Both the optical[23] and electronic[24] properties of thin films of the pristine polythiophene derivatives are known to improve with increasing degree of RR. The side chains in the RR form tend to stack into planar structures known as 'lamellae', which may adopt two different orientations, namely, parallel and normal to the substrate, depending on the processing conditions and regioregularity.[25] Higher RR along with longer side chains enables closer packing of these lamellae such that the optical[24] and electronic[23] excitations adopt interchain character. Such well-ordered self-assembled lamellae formation is, however, absent in the regiorandom analogue of the polymer and is believed to be responsible for the distinct shoulders observed on the long-wavelength side of the absorption maximum and for the large red-shift of the absorption maxima in the regioregular derivatives shown in Figure 4. Previously, we have shown that the Faraday rotation from thin spun coat films of alkyl and alkoxy substituted polythiophene derivatives strongly depends on the regioregularity.[8] Here we show that the Faraday rotating ability of these polymers is strongly influenced by their supra-molecular organization within the thin films and strongly dependent on the processing conditions.

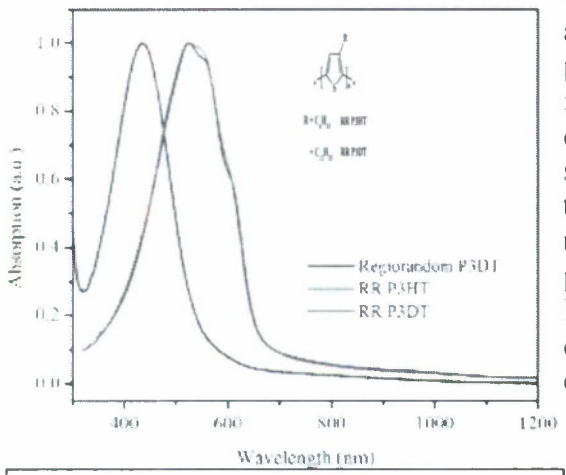

Figure 4. UV-Vis absorption spectra measured from thin films of P3DT, RRP3HT and RRP3DT. Inset shows the molecular structures of the polymers under investigation.

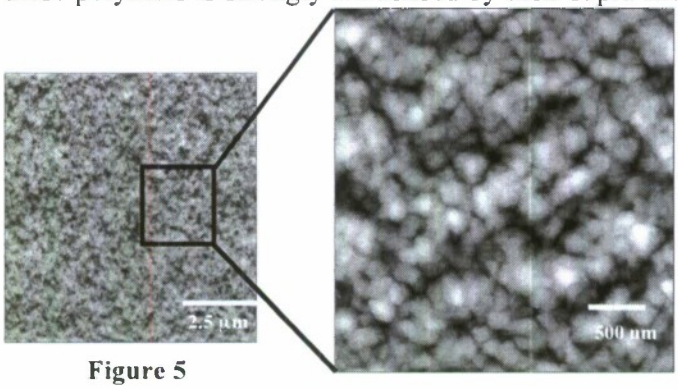

Figure 5

The crystalline mesoscale morphology in the spun coat film's lateral direction was investigated using AFM. Figure 5 shows a representative AFM contact mode topographic image of an RRP3DT film spun cast on a Si substrate. The large scale image (10 μm × 10 μm) shows a homogeneous top surface of about 1 μm thick film with rms surface roughness < 6 nm. The zoomed topographic image shows a structured top face of the film with weak signature spherulitic structures. Note that the commonly observed nanometer scale fibriller crystalline structure in polythiophene derivatives is absent.[25] Previous studies based on rapid thin film deposition have shown a highly ordered rod like structure for films with relatively low MW of 3.2 kD.[26] However, we found that very little difference can be observed in films spin cast from different solvents, such as chloroform, toluene, *p*-xylene etc., and thicknesses ranging from 0.5 μm to 1 μm, all having similar amorphous and granular surface topography by AFM.

Table 2. V, Verdet constant (10^4°/T-m) of polymers RRP3DT and RRP3HT measured at different wavelengths. Typically 200 nm to 1 μm films are used for these measurements. Standard deviations calculated from multiple independent measurements are shown in the bracket.

	532 nm	633 nm	670 nm	980 nm	1310 nm	1550 nm
RRP3DT	+ 2.06 (0.3)	+ 2.6 (0.6)	+ 2.2 (0.2)	+ 1.6 (0.3)	+ 1.2 (0.2)	+ 0.85 (0.04)
RRP3HT (Spun coat)	+ 6.25 (0.3)	+ 4.42 (0.2)	+ 4.02 (0.2)	+ 2.01 (0.04)	+ 1.04 (0.2)	+ 0.84 (0.03)
RRP3HT (Melt Processed)	-	-	+ 0.60 (0.002)	+ 0.43 (0.003)	+ 0.21 (0.001)	-

Faraday rotation measurements were carried out on multiple spun coat films of RRP3DT, RRP3HT and their regiorandom counter parts. The Verdet constants calculated from the measured Faraday rotation are shown in Table 2. The regiorandom derivatives are either Faraday inactive or the rotation is below the detection limit of our system. Within measurement error both the polythiophene derivatives show quite similar Faraday activity. To further investigate the dependence of Faraday rotation on the crystallinity and the lamellae type structure of these polymers, films were subjected to different processing conditions followed by rigorous Faraday rotation measurements. Polymer crystallization into a film from solution is a very complex exothermic process largely controlled by the thickness along with other factors such as solubility, spin casting temperature, heat transfer coefficient, heat capacity etc. The crystallinity and crystal domain orientation of such films are known to be dependent not only on regioregularity and molecular weight, but also on the processing conditions.[27]

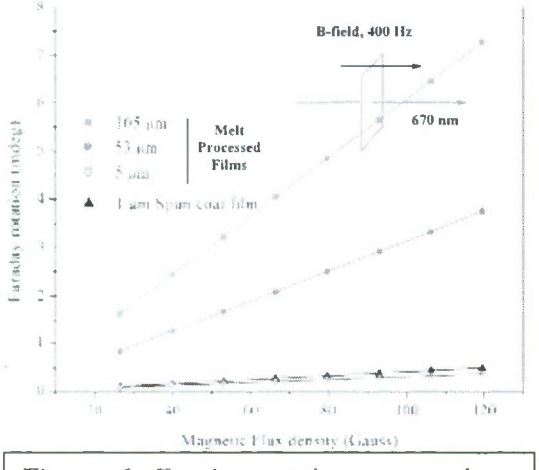

Figure 6. Faraday rotation measured on spun coat and melt processed films of RRP3HT. Film thicknesses and data collection geometry are indicated.

In order to alter the crystallinity of the spun coat films we subjected the spun coat films (i) to melting at a temperature 30°C higher than the melting points of each polymer and subsequently cooled to room temperature at a slow rate of about < 1 °C / minute and (ii) to melting at a temperature as in (i) with subsequent quick quenching at – 77 °C. Faraday rotation disappeared completely from the films of both RRP3DT and RRP3HT prepared using the method described in (ii). We have also observed that Faraday rotation from 1 μm thick films of RRP3DT decreases dramatically upon melt processing following (i), to barely above the detection limit of our setup. Disappearance of the "shoulders" in the absorption spectra from these films indicates a possible collapse of the lamellae structure. However, Faraday rotation

from melt-processed films as prepared and from spun films of RRP3HT could be measured and the results are shown in Figure 6. An important advantage of melt processing is that the process yields good optical quality films with large thickness (tens of microns), quite difficult to achieve with spin coating for this class of polymer. Although the Verdet constant measured from melt processed films of RRP3HT is considerably lower (~ 6000 °/Tm at 670 nm) than that of the spun coat films (~ 40000 °/Tm at 670 nm), it is easier to achieve larger rotation from melt processed thick films, a key element in any MO applications such as, isolators or magnetic field sensors. Determination of the sign of the Verdet constants measured from the thin films of RRP3HT and RRP3DT required more rigorous analysis of the changes in phase than for a pure material, such as BK7 or TGG. Careful comparison of phase information recorded on thin films of several different thicknesses at appropriate wavelengths and different input polarizations (such as, 45°, 135°, 225° and 315°) revealed that both polymers had Verdet constants with the same sign as the substrate, BK7. In the case of RRP3HT the sign of the Verdet constant determined from a melt processed free standing film of 53 μm thickness was found to be same as that of its spun coat films. Since the sign of the Verdet constant is believed to be an intrinsic materials property it can be expected that the sign will be independent of the processing conditions.

Room temperature X-ray diffraction patterns of the processed RRP3DT and RRP3HT films are shown in Figure 6. The X-ray diffraction pattern of the RRP3DT spun coat film shows distinctive peaks at 2θ = 3.8 (100), 7.5 (200) and 11.4 (300) corresponding to *d* spacing of 23.5 Å for the interchain distance between two neighboring polythiophene chains within the lamellar structure. The RRP3HT film shows peaks at 2θ = 5.8 (100), 11.5 (200) and 16.8 (300) corresponding to *d* spacing of 14.2 Å. Lamellar structural orders of this type had earlier been observed in regioregular polythiophenes.[28] Since the *n*-dodecyl and *n*-hexyl chains are ~13.5 Å and ~6.8 Å long respectively and are tilted at ~50° against the backbone in the coplanar polythiophene conformation,[29] the d-spacing values suggest that both RRP3DT and RRP3HT have significant amounts of interdigitation, stronger in the case of RRP3DT. Decreased diffraction intensity and narrower half width from the films processed through melting and subsequent slow cooling are indicative of collapsed lamellae structures, but with somewhat larger crystal domains. However, the films processed through melting and quick quenching at – 77 °C do not show the presence of any crystallinity whatsoever indicating a complete collapse of the lamellae structure in these films. Differential scanning calorimeter data (not shown here) in the case of dodecyl side-chain substituted polymers indicates that there exists an irreversible phase change around ~ 80 °C which is absent in the case of shorter side-chain groups, such as in RRP3HT. Whereas the collapse of the lamellar structure is a universal phenomenon upon melting and quick quenching at -77 °C, irrespective of side chain length, the

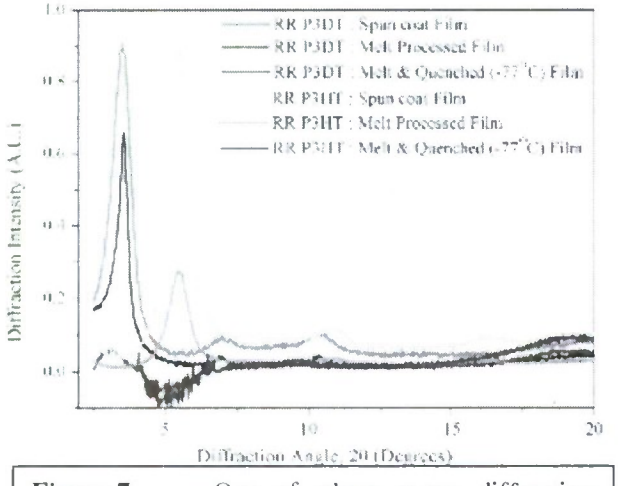

Figure 7. Out of plane x-ray diffraction profile of RRP3DT and RRP3HT thin films prepared under different conditions. The geometry of the data collection is indicated.

phase change above 80°C seems to be a critical factor influencing Faraday rotation in the case of RRP3DT.

4.1.5 Mechanistic approach

We now discuss possible candidate mechanisms for the large Faraday rotation observed from the conducting polymers reported here. To the best of our knowledge, the mechanism causing MO activity in these polymers is not known. In most inorganic crystals and glasses Faraday rotation derives from the presence of a significant density of free spins associated with magnetic ions containing triplet energy states, a mechanism that is not applicable to our polymers. In these so-called "paramagnetic transitions" the time average of microscopic magnetic moments is non-zero at room temperature and is not time reversal invariant.[10]

The basic mechanisms responsible for MO activity observed in diamagnetic materials are: 1) diamagnetic transitions,[11] 2) interband effects within spin-split Landau levels,[30] 3) positive free carrier rotation[31], and 4) dynamic spin organization of magnetic polarons generated due to defects in semiconductors.[32] In the electric dipole optical transition regime, the classical diamagnetic transition generally addresses the difference in oscillator strength experienced between the right and left circularly polarized light interacting with the excited multiplet caused by Zeeman splitting. The Zeeman energy, given by $\Delta E = g\mu_B B$, where g is the Landé g factor (~ 2 for organics) and μ_B the Bohr magneton, is only of the order of 1 μeV at a field of 100 gauss, and therefore much smaller than the thermal energy kT at room temperature. Faraday rotation derived from degenerate Landau levels follows a mechanism similar to the diamagnetic transitions found specifically in semimagnetic semiconductor systems and can be estimated from the balance of thermal and Zeeman energy. Thus, neither of these two mechanisms explains the large Faraday rotation found in the regioregular polythiophenes.

Faraday rotation due to positive free carriers is the dispersive consequence of the cyclotron resonance of the conducting electrons under applied magnetic field. The magnitude of the free carrier rotation is on the order of $\sim N\xi^2 B / \lambda^2$ where N is the number of free carriers and ξ is the mobility.[33] At 100 gauss, using a typical value for the mobility, $\xi \sim 10^{-4}$ cm^2/Vs[34] and with a carrier concentration of $\sim 10^{15}$/cm^3,[35] we estimate the Verdet constant as on the order of 10^{-4}, which is therefore much too small to explain the magnitude of rotation observed. Furthermore, none of the heretofore discussed mechanisms are known to be dependent on supramolecular structure formation. Electron paramagnetic resonance experiments show that these regioregular polythiophenes contains only 10^{-5} spins / chain making them virtually defect free compared to the magnetic polarons found in dilute semimagnetic semiconductors.[12] However, direct photogeneration of an optical exciton or polaron pair presents an interesting possibility.[36] These excitons / polaron pairs are known to be strongly dependent on the interchain interactions present in the thin films of π-conjugated polymers, such as the regioregular alkyl substituted polythiophenes. The energy equivalence of the magnetic dipole fields between polaron or exciton pairs are expected to be of the order of 100 gauss which also suggests the possibility of forming spin containing units under such low magnetic field excitations. Possibilities of stronger spin-orbit coupling arising from such spin containing units not only supports our observations of Faraday rotation in these thin films under low magnetic fields and continuous wave excitation, but also explains their dependence on the lamellae type organization and strong interchain interactions.

Another plausible mechanism is the possibility of coexistence of partially flat and dispersive bands in these strongly correlated electronic systems. π-conjugated polymers with

relatively shorter chains are known to have strong itinerant electron correlation and high mobility. It has been theoretically shown[37] previously that such a system may have a strong tendency towards ferromagnetism. Recently we have confirmed that pristine RRP3DT does possess a ferromagnetic phase with a Curie temperature of ~ 20 K.[38] Even a weak magnetic field applied to the ferromagnetic phase is enough to drive the system into significant magnetization / spin polarization, enhancing the magnetic susceptibility but maintaining the non-magnetic status of the bulk material. With diminished thermal energy and magnetic excitation, a majority of the spins can be shifted to the dispersive part of the band, possibly resulting in Faraday rotation involving ferromagnetic transitions, higher conduction or negative magneto-resistance under small magnetic fields. Such a conjecture can be supported with the recent observation of negative magneto-resistance at low temperature in the case of RRP3HT.[39] However, ferromagnetism is not an essential condition for either negative magneto-resistance or Faraday rotation and at higher temperatures the balance between transport and spin structure may fall apart. Another disadvantage of such a picture is that this model does not address the issue of lamellae type supra-molecular organization and thus may not be fully applicable to our systems. We plan on further investigating the magnetic properties of the regioregular polythiophenes while also pursuing femtosecond time-resolved photoluminescence studies to ultimately elucidate the origin of the large Faraday effect in these materials.

4.2. Magnetic properties of polythiophene derivatives

Despite intense effort for over two decades aimed at developing alternatives to traditional magnets, robust ferromagnetism in organic polymers has been elusive.[40] These materials are of unparalleled technological importance as they can potentially be used as plastic magnets and magneto-optic devices with the advantage of the flexibility of organic chemistry by allowing for further tuning of their properties.[41] Physical realization of such a magnetically ordered polymer system involving only π-electrons is a rare occurrence.[42] Various strategies for synthetic tailoring are being investigated to establish the optimized supramolecular structure and packing required to maximize magnetic order.[43] Possibilities for polaronic ferromagnetism have been explored in doped π - conjugated polymers.[44] Recently the concept of band ferromagnetism in π - conjugated polymers that exploits the itinerant nature of their π - electrons and structural frustration of electron transfer has been proposed theoretically.[45] Although unstable at ambient conditions and thereby not viable for large scale applications, ferromagnetic order temperatures on the order of 0.2 to 40 K have been achieved in carefully designed organic polyradicals with long range order.[46] An average spin as high as S = 5400 has been achieved in this class of polyradicals.[47] Here we report on the observation of low temperature magnetic ordering of a purely organic polymer, regioregular (RR) poly(3-dodecyl)thiophene (P3DT, **1**, Figure 1A) in its pristine state.

Magnetic studies of various polythiophene derivatives, doped and pristine, have been reported previously.[7,48] Although it is known that regioregularity improves both optical and electronic properties of pristine polythiophene derivatives, it has never been addressed with respect to magnetic properties.[49] RR polythiophene chains stack into an organized three-dimensional structure giving its optical and electronic excitations some interchain character.[10, 50] In polymers with a relatively low degree of polymerization flatter thiophene ring configurations and longer π-conjugation length are facilitated, further increasing at lower temperature.[51] Our magnetic polymer, poly(3-dodecyl)thiophene (P3DT, **1**) is designed to have a length of 70 monomers with regioregularity for the chain (without the head-group) > 99% as obtained from

NMR. Regiorandom P3DT (**2**, with 50% H-T coupling) of similar molecular weight was used to compare the effects of regioregularity. To our surprise we found that **1** forms doughnut shaped nanostructures (Figure 8) unlike the rod and worm shaped structure previously reported albeit with larger chain lengths (> 200 monomers).[52] An atomic force microscopy (AFM) topographic image shows that the toroid forming the doughnut has a maximum of 9.2 nm and 22 nm as its tube outer and inner diameters, respectively. Although doughnuts with smaller dimensions were present, no other shape was observed. **2** was found to form fibrous structures under similar sample preparation conditions. On investigation of its magnetic properties, we found that **1** has a low temperature magnetically ordered phase (Weiss temperature, θ = 10.2°K) which is not only stable under ambient conditions but also has a very large spin quantum number, whereas **2** was found to be barely paramagnetic.

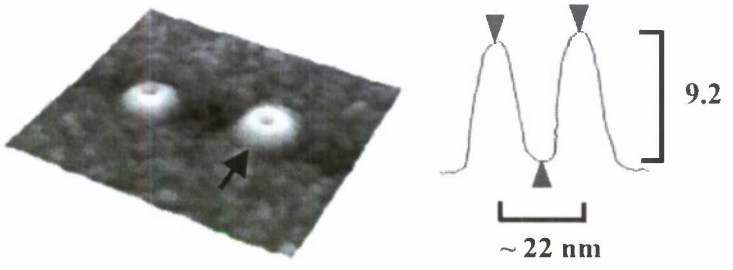

Figure 8. False color AFM topographic image of RR-P3DT doughnuts. The scan line is a vertical cross section of the doughnut indicated by an arrow.

The magnetic field (H) dependence of magnetization (M) measured at several temperatures (T = 1.8°K - 20°K), shows a very fast rise at low H and reaches near saturation at fields as low as 3 Tesla (Figure 9). Numerical fits of the M versus H/T data at 4.5°K to a percolation model give an average spin quantum number (S) of 8315.[13, 53] However, S values and saturation magnetizations calculated at different temperatures do not scale with temperature, a behavior expected for a conventional ferromagnet. The non-ideal Curie-Weiss type behavior with $S \approx 8000$, gives an approximate estimate from an effective ferro- or ferrimagnetic correlation among electron spins. Assuming physically realistic, predominantly antiferromagnetic interactions among the itinerant π-electrons and between two nearest neighbor chains, this can represent a lower bound estimate on the number of correlated electrons.

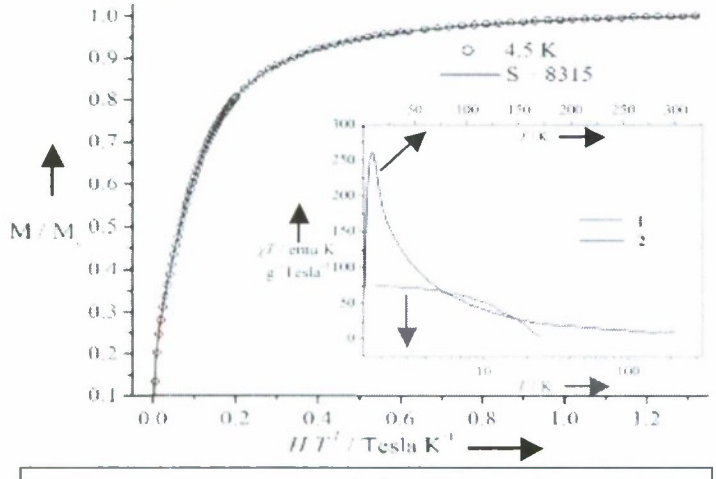

Figure 9. Magnetic field (H) dependence of the magnetization (M) of polymer **1** at 4.5°K, plotted as M/M_s versus H/T where M_s is magnetization at saturation. ***Inset:*** Plots of χT of **1** and **2** versus T (top and bottom axes) where χ = M/H is the measured dc-susceptibility.

In the Figure 9 inset, the product χT ($\chi = M/H$, dc susceptibility) of **1** and **2** are plotted as a function of T. In the case of **1** above 30°K, χT decreases slowly, reflecting a weakly varying χ, likely due to paramagnetic behavior. However, below 30°K, χT increases sharply as expected from the onset of ferromagnetic correlation precursive to a transition at T_c = 16°K. χT

was found to be highly field dependent, typical of a system with a large magnetic moment. The maximum at 6°K and subsequent decrease at lower temperature is a consequence of moment saturation below the Curie temperature and indicates blocking of the magnetization. The absence of high temperature susceptibility with $\theta > T_c$, though unusual for a traditional local moment ferromagnet, can be found in itinerant ferromagnets.[8,54] **2** was found to possess weaker susceptibility at low temperatures and could not be measured at temperatures > 25°K. Although the possibility of an ordered phase below 1.5°K (instrumental limit) cannot be ruled out, clearly, the magnetic properties of **2** are very different from those of **1**.

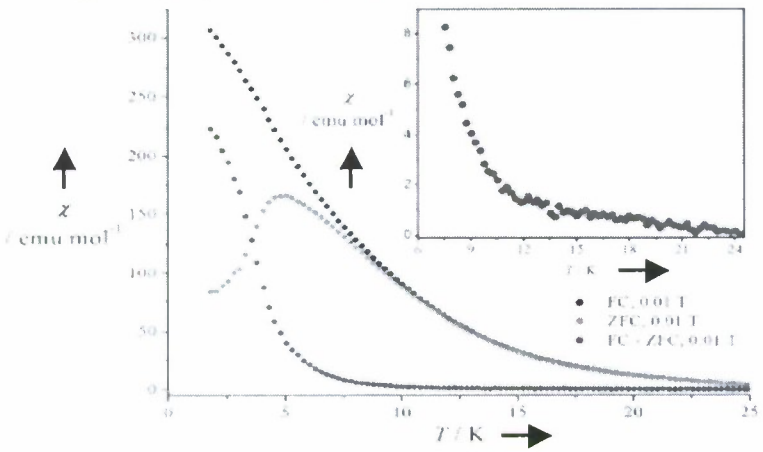

Figure 10. ZFC and FC susceptibility data of **1**. ***Inset:*** The differences between FC and ZFC magnetization in the temperature range of 6 – 24°K are shown.

The temperature dependence of χ in **1** at low applied field (0.01 Tesla) reveals that the zero field cooled (ZFC) and field cooled (FC) magnetizations diverge below 21°K (Figure 10), again indicative of ferromagnetic correlation. Figure 11 shows magnetization hysteresis loops of polymers **1** and **2** at 1.8°K measured in the field range of ± 3 Tesla. Saturation of the bulk magnetization is clearly seen over 2 Tesla of applied field. The large remnant magnetization and hysteresis in **1** are suggestive of strong ferromagnetic ordering. However, in **2**, within the experimental uncertainty of ± 2 Oe, there is no hysteresis with zero coercivity and remanence, which is a typically paramagnetic behavior. A closer inspection of M(H) of **1** at various temperatures below T_c reveals that M is linear only at low values of H. ΔM (see inset of Figure 11), is defined as the magnetization range over which M is linear with H, that is ΔM is directly proportional to the spontaneous magnetization. The plot shows that ΔM drops sharply with increasing temperature, a behavior unexpected for a strong ferromagnet. For superparamagnetism, M is known to scale as H/T, unlike what is seen in **1**.[55] As for reference, a ΔM value of 1.1 emu/g at 3.5°K corresponds approximately to a moment value comparable to $S \approx 8000$. The magnetic moment diameter calculated from the ΔM values at low H field and at 5°K is ~ 12 nm, comparable to the dimensions of the doughnuts of **1** measured using AFM[56] and the grain size measured using small angle x-ray diffraction.[**Error! Bookmark not defined.**]

To further investigate the nature of magnetic ordering in **1** we carried out ac-susceptibility measurements. The relaxation of the magnetization for **1** at low temperatures is best observed in the temperature and frequency dependence of the in-phase component of the ac-susceptibility (χ', Figure 11). The peak maximum in χ' at T_m' shifts to lower temperatures and it gains in amplitude with decreasing frequency. The value of $\Delta T_m'/(T_m' \Delta(\log w)) \approx 0.06\text{-}0.07$ indicates the change in the blocking temperature with the angular frequency (ω), suggesting that the relaxation behavior is very similar to that of an insulating spin glass.[57] However, the out-of-phase ac-susceptibility (χ'') shows less pronounced frequency dependence than χ', indicating that

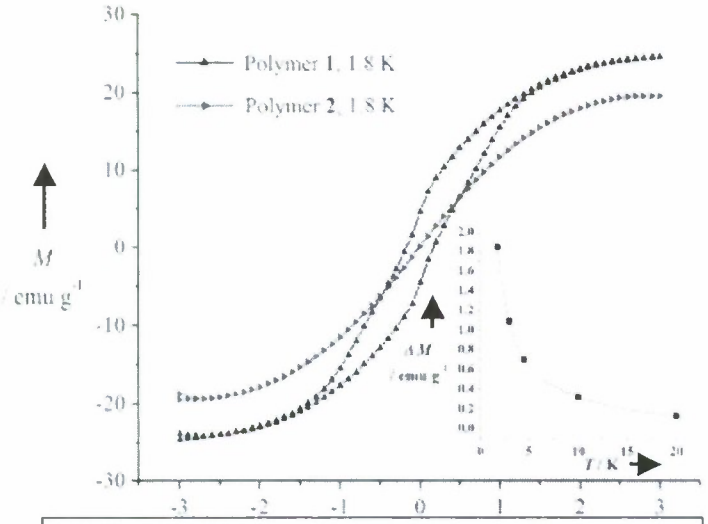

Figure 11. Magnetization of polymers **1** and **2** is plotted as a function of magnetic field at 1.8 K. ***Inset***: ΔM versus temperature: solid line is just a guide to the eye (see text for details).

the magnetic moments are of an interacting nature.[58] The Figure 12 inset shows the plot of $\ln\tau$ versus $1/T_m'$ where $\tau = w^{-1}$ is the relaxation time of the magnetization and T_m'' is the temperature relating to the χ'' peak. The energy barrier (E_A) associated with the blocking and the magnitude of τ can be estimated from this plot following the Arrhenius law, $\tau = \tau_0 \exp\{E_A/k_B T_m''\}$. Within the narrow frequency range of our measurements, the plot fits to a straight line (R = 0.997) and with an order of magnitude estimate we have $\tau_0 = 7.8$ *nsec* and $E_A/k_B = 72$°K the system behaves as an ordered spin glass.[59]

The exact origin of the magnetic ordering in **1** remains an open question. Electron spin resonance measurements show a spin concentration of 5×10^{13} spins/g in **1**.[60] Such a low spin concentration cannot account for the susceptibility of **1**. We believe that the nano-confinement of itinerant π-electrons of RR polythiophene in an anisotropic structure such as a doughnut may be the main origin. With thermal chaos down to a minimum, spontaneous alignment among the toroidal moments generated from the nano doughnuts is a strong possibility for creation of magnetic ordering in P3DT.[61] The role of frustration in spin polarization on sulphur in thiophene rings and increased $d\pi$-$p\pi$ spin orbit interaction[62] in overall magnetic ordering is another intriguing possibility. Another plausible mechanism is the possibility of coexistence of partially flat and dispersive bands in these strongly correlated electronic systems, resulting in so-called 'flat band ferromagnetism', suggested recently.[6] Such a conjecture can be further supported by recent observation of negative magnetoresistance at low temperatures in a shorter chain polythiophene derivative.[63] On the other hand, at low temperature the entire 3D organization typical of RR polythiophene may have collapsed causing self doping and defect induced residual magnetism. We are at present performing a detailed comparative study of structural, magnetic and electronic properties of **1** in order to determine more precisely the origin of the magnetic behavior reported here. To our knowledge, there is no other purely organic stable polymer system reported to

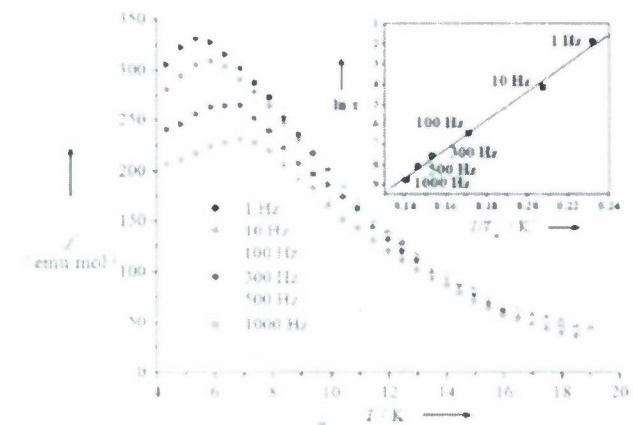

Figure 12. Temperature dependence of the *in-phase* ac susceptibility χ' at ac driving field of 5 Oe is shown. The measurement frequencies are indicated. ***Inset***: Arrhenius plot of the natural logarithm of relaxation time as a function of $T_m''(K^{-1})$.

date that displays magnetic ordering in the nano regime.

4.3. Acrylate polymer/magnetite nanoparticle composite – synthesis, poling and MO properties.

An entirely different approach to achieving the required Verdet constants is to synthesize a polymer nanoparticle composite. We chose magnetite nanoparticles, which are super-paramagnetic and commercially available with tremendously well-controlled and narrow size distributions (15nm and 10 nm). The basic design strategy is shown in Figure 13, where we start with a suspension of acrylate monomer, stabilized magnetite nanoparticles and solvent. The acrylate monomers actually physisorb on the magnetite particle surface, which sets the stage for the growth of a polymer shell around the particle upon photoexcitation. The resulting polymer coated magnetite nanoparticles then become embedded in the acrylate polymer host after subsequent thermal polymerization. This approach achieves excellent nanoparticle dispersion by both taking advantage of entropic forces in the initial mixing and energetic factors subsequent to polymer coating, while the host polymer properties can be substantially varied by choosing different acrylate monomers.

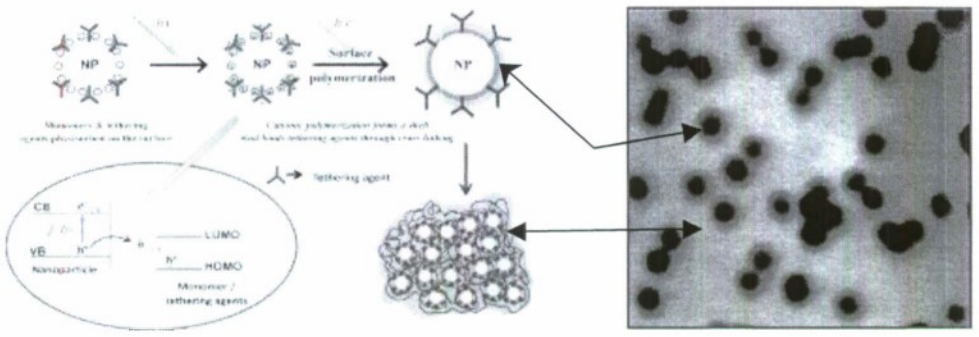

Figure 13. ***Left.*** Schematic description of nanoparticle / nanotubes–polymer core– shell nanocomposite formation. ***Right.*** Scanning transmission electron micrograph of a core – shell magnetite nanoparticle – PMMA nanocomposite.

We have used both transmission electron microscopy (TEM) and scanning transmission electron microscopy (STEM) to examine the magnetite nanoparticles themselves and the composite as shown in Figure 14. On the left we see the phenomenal particle size distribution of this composite; we can also see that the particles are very nearly uniformly spherical. The STEM of the composite shows that the particles are largely nonaggregated and discrete, as required to minimize scattering losses.

Initial measurements of the Verdet constants of these materials were promising, showing values equal to or greater than those of the polythiophenes with far superior processability for only a few% by volume loading. We then realized that we might be able to achieve truly exceptional performance by using an external magnetic field to orient the particles in the polymer at elevated temperatures and then allowing the composite to cool with the field applied. Figure 15 shows the apparatus that we used for this process and the difference between the films color before and after poling.

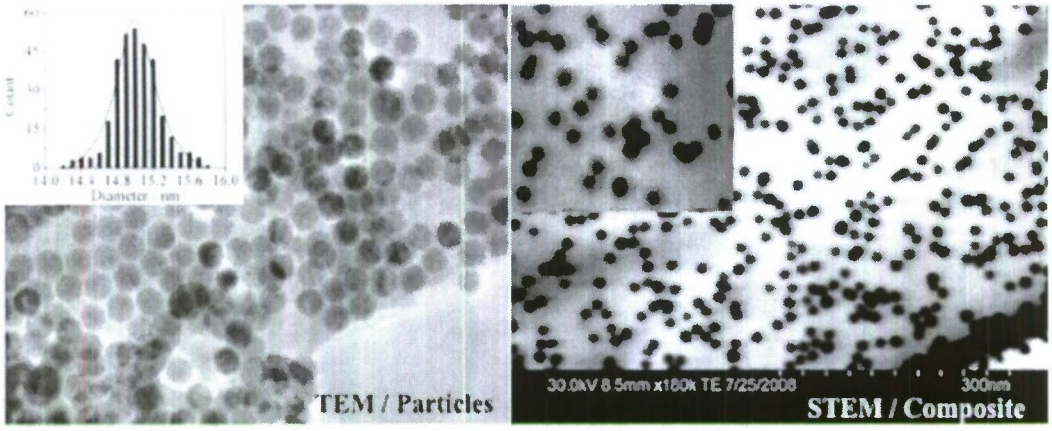

Figure 14. TEM and particle size distribution for magnetite nanoparticles (***left***); STEM of the acrylate polymer/magnetite nanoparticle composite (***right***)

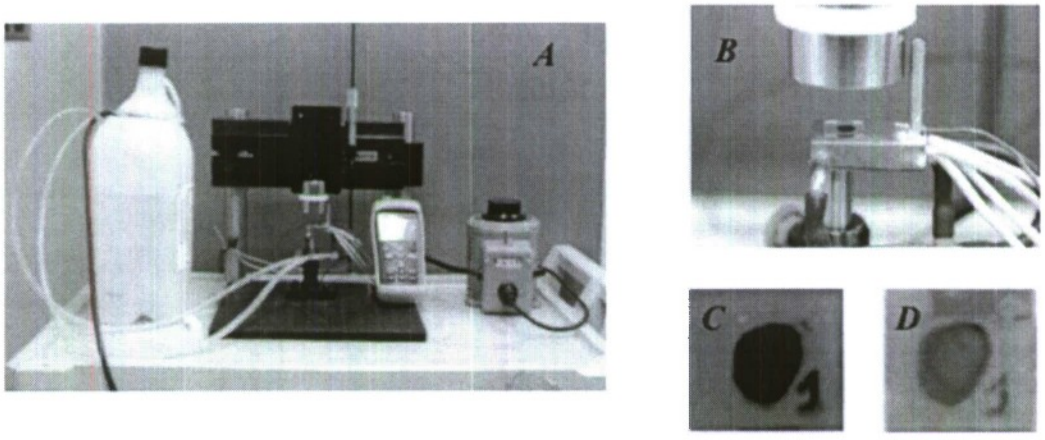

Figure 15. (**A**) Magnetic field poling station; (**B**) Close-up of the poling region showing heating elements; (**C**) Isotropic nanocomposite film; (**D**) Poled film showing poling induced reduction in absorption

The benefits of the poling process are shown in Figure 16, where we plot the measured Verdet constants for polymer nanocomposite films vs. the volume fraction of magnetite nanoparticles for pristine and poled films. Note that the accuracies of these measurements are significantly higher than those for the polythiophenes as we were able make nanocomposite films tens of microns thick. We see that the poling process increases the Verdet constant by factors of 4-5, resulting in a Verdet constant of 22×10^5°/T-m (at 980nm), which is as large or larger than the best garnet material. The decline at higher concentrations may indicate a percolation phenomenon or increased aggregation.

4.4: Waveguide Loss Measurements

In the course of waveguide isolator design and fabrication we have performed waveguide loss measurements using direct measurements of insertion loss as well as cutback techniques as discussed above. In addition we have a liquid prism slab loss measurement system that allows us to measure slab waveguide losses as low as 0.1 dB/cm at 1550nm or 1310nm. We have used

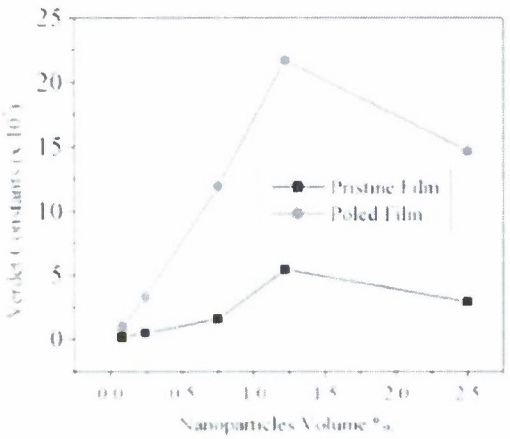

Figure 16. Verdet constant of both poled and pristine nanocomposite film as a function of nanoparticle volume percentage.

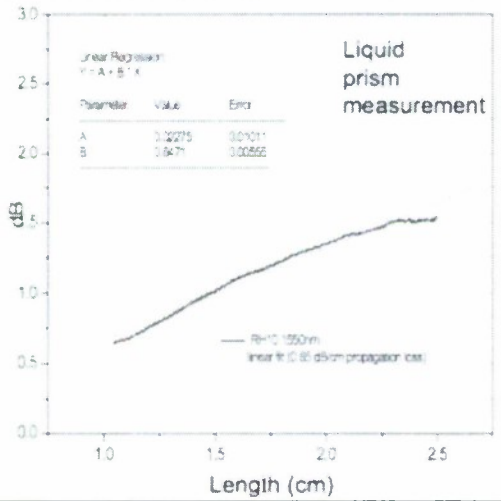

Figure 17. Liquid prism slab waveguide loss data for low-loss sol-gel RH10.

this system to assist us in our development of lower loss sol-gel materials. To reduce loss due to C-H and O-H vibrations in the 1550nm window we have adopted a new formulation method that uses a stoichiometric quantity of water (as opposed to an excess) and we have incorporated sol-gel precursors with reduced aliphatic C-H content. One of the benchmark formulations in this new paradigm is RH10, which is 25 mole% methacryloyloxy propyltrimethoxysilane, 25 mole% phenyltrimethoxysilane and 50 mole% diphenyldimethoxysilane. The TE slab waveguide loss at 1550nm for a thin film of this material is shown in Figure 17, where we see a loss of 0.65dB/cm, which represents an improvement by a factor of 2 to 3 over materials that we are currently using for waveguide isolator development (SU-8 – 1.3dB/cm loss at 1550nm). SU-8 is convenient as it is commercially available as a resist and has excellent photolithographic contrast, whereas the new lower loss sol-gels are still being optimized for photolithography. A sol-gel with a refractive index of about 1.53 at 1550nm has been used for our waveguide Faraday rotator demo that is described below. We plan on evaluating commercially available acrylate formulations from the company ChemOptics, as they have materials that claim losses nearly as low as 0.1 dB/cm and tunable refractive indices, which are absolutely necessary for optimizing the waveguide isolator performance.

4.5 Waveguide Faraday rotator demo

As discussed above Faraday rotation is the strongest MO effect and its realization in integrated waveguide devices promises to achieve such features as compactness, polarization insensitivity, etc. In order to have a waveguide that exhibits Faraday polarization rotation, the following conditions should be met:

1. Equal propagation constants for both TE and TM eigenmodes
2. Single mode propagation
3. Orientation of the chirality axis parallel to the waveguide propagation direction

In order to meet Requirement 1, we developed a technique for

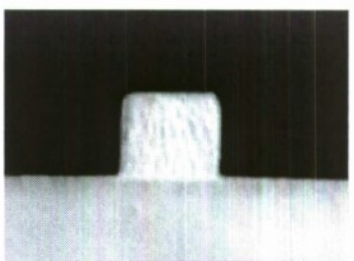

Figure 18. Square waveguide made in SU-8

making waveguides with nearly perfect square cross-sections as shown in Figure 18. This symmetric core was then coated with the acrylate polymer/magnetite nanoparticle composite polymer thus providing the same index difference ($\Delta n=0.008$) on three sides of the waveguide cross-section. The refractive index difference on fourth side (between the waveguide bottom and the glass substrate) was larger ~ 0.002. Full WG symmetry can be achieved using either a buffer layer with a refractive index equal to that of the polymer or by using a substrate with an index close to the target and by varying the height of the core to equalize the TE and TM propagation constants.

Single mode propagation (Requirement 2) was achieved by varying the size of the waveguide cross-section for a given refractive index difference, and we settled on 5 x 5μm^2. The proper orientation of the MO polymer nanocomposite was achieved by poling the nanocomposite. In this case, a novel poling technique was developed whereby the MO cladding was deposited and dried under a magnetic field, enabling us to avoid high temperature processing of the device, which could potentially damage the waveguide core and the magnets (see Figure 19). The polarized output from DFB 1550 nm laser was used to excite TE and then the TM mode of the sample. The output was collimated and then projected on an IR camera through a Glan-Thompson prism to monitor the change in polarization. The measurement system was aligned in such a way as to be able to insert in real time toroid type magnets around the waveguide to impose a variable magnetic field along the waveguide. The measurement system also allowed us to reverse the orientation of the magnetic field to see if the polarization rotation switches its sign, proving that the polarization change corresponds to Faraday rotation. We observed ~2° Faraday rotation that was independent of input polarization. The rotation appeared only when we applied a non-homogeneous magnetic field along the waveguide with the maximum at its edge. This shows that there was not quite enough synchronization between TE and TM modes (as described above) since any excitation of the probe orthogonal mode is canceled in a homogeneously applied magnetic field and a small value of the probe beam can be observed with a localized magnetic field (on the edge in our case). This result clearly shows that equal propagation constants of WG eigenmodes is a key parameter to be optimized and we expect to enhance it in our devices by their proper symmetrization as described above.

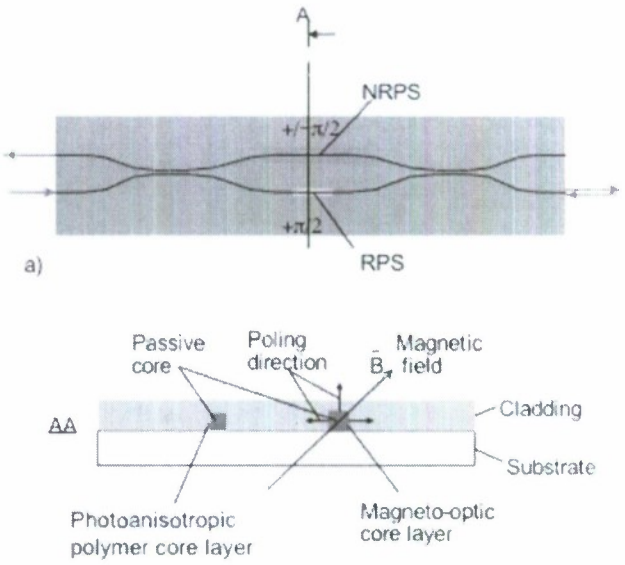

Figure 19. Schematic of the waveguide isolator showing key subcomponents.

4.6 Magnetic Field Sensor

Magnetic sensors have a wide range of applications that include military and surveillance (e.g magnetic anomaly detection), navigation, nondestructive evaluation, current sensing, magnetic media characterization and medical/biological imaging.[64] Among these, optical

sensors offer several advantages including immunity to electromagnetic interference, excellent sensitivity, fast response time, and high spatial resolution. MO sensors are based on the Faraday effect, that involves the rotation of the plane of polarized light when traveling through an MO material. We have developed an all-fiber stand-alone setup that can be used to screen different materials for their magnetic field sensing ability. Along with polymer based materials we have also investigated several garnet based crystals for potential magnetic field sensing applications. In the next section we briefly describe our work on one of the garnets that have been investigated. Garnets are generally ferromagnetic in nature and the angle of rotation θ in a ferrimagnetic or ferromagnetic material is given by $\theta = B\theta_S L\cos(\alpha)/B_{sat}$ where B is the applied magnetic flux density, L is the optical length through the MO material, θ_S is the specific Faraday rotation of the material, B_{sat} is the saturation magnetic field and α is the angle between the direction of propagation of light and the internal magnetization of the material. Sensors based on the Faraday effect in gallium-substituted yttrium iron garnet crystals with a noise-equivalent magnetic field sensitivity of 100 pT/√Hz at 500 Hz and frequency response extending up to a GHz have been previously reported.[65]

4.6.1. Magnetooptic Garnet Films with Planar Uniaxial Anisotropy

Ferrimagnetic bismuth rare-earth iron garnets used in traditional isolator and switching applications have high specific Faraday rotations and excellent transparency at infrared telecommunications wavelengths. These materials are grown by liquid phase epitaxy typically on (111) rare earth gallium garnet substrates, resulting in the magnetization being constrained to be parallel or antiparallel to the growth direction. The demagnetized configuration is serpentine stripe domains of alternating magnetization and the magnetized configuration is a single saturated domain. Traditionally, these materials are used in non-reciprocal optical devices where the light is propagated perpendicular to the major faces of the garnet and parallel to the growth direction. Perpendicular propagation devices require perpendicular magnetic fields and magnetization processes. Such sensors with perpendicular light propagation are constrained by the speed of domain wall motion, and the maximum achievable film thickness limits their ultimate sensitivity. Recent developments[66] have produced thick film Faraday rotators grown on (100) substrates with specific rare earth combinations that yield a negative or planar uniaxial anisotropy. In the plane of such negative anisotropy films, there is almost no energetic barrier to domain rotation. In-plane propagation of light in planar anisotropy magnetic garnet films can take advantage of these speeds and sensitivities and offers the possibility of much longer path lengths for high-sensitivity, high-speed MO sensors, switches and modulators. However, the coupling of light to such a small clear aperture presents problems and the films must be grown with a much higher degree of compositional uniformity along the growth direction to prevent lateral gradients in the index of refraction that would bend and distort the beam.

The $(BiGdLu)_3(FeGa)_5O_{12}$ films prepared for this application have a specific Faraday rotation θ_S of 0.09 °/mm and specific absorptions α of 0.05 mm^{-1} at 1310 nm; however there are additional losses from coupling and beam spreading. The as-grown film on the substrate was cut into square slabs and the substrate was ground and polished away to leave a free standing film. Two opposite edges of the slab were polished and the slab was then cut into strips 14 mm in length by 0.5mm^2.

4.6.2. Magnetic Field Sensor

As described in section 4.1.2, we have accurately characterized Faraday rotation in polythiophene thin films using a free-space polarimeter setup. The high sensitivity magnetic field sensor reported in this paper employs a 1310 nm superluminescent diode (SLD) source, a five-axis positioning system for aligning the MO slab with fiber, PM fiber and optics for

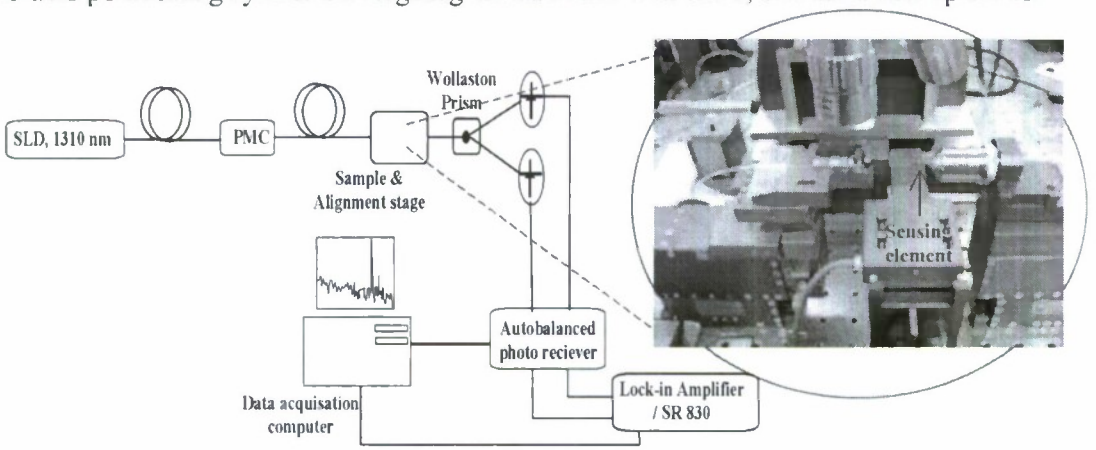

Figure 20. Block diagram of the magnetic field sensor setup. Inset shows setup for aligning garnet slab with 1310nm fiber.

polarimetric detection, and an autobalancing laser noise cancellation photoreceiver to detect small changes in Faraday rotation. The sensor setup shown in Figure 20 includes a polarization controller at the output of the SLED to provide desired linearly polarized light, a low-NA microscope objective for capturing the light output from the sample, a Wollaston prism (extinction ratio of 1:500,000) to separate the two linearly polarized components of the output which are subsequently detected by two auto-balanced detectors, and a dual phase lock-in amplifier (SR 830). Auto-balanced phase sensitive detection is used to reduce common mode laser noise using the method of comparing one or more signal beams to a reference beam. The small cross-sectional dimensions of the garnet slab and small-area detectors used in the autobalancing photoreceiver make the setup sensitive to light intensity fluctuations due to vibrations and air-currents, which in turn can limit the ultimate sensitivity. An index matching fluid was used at the fiber-slab interface to minimize coupling loss and yield a stable optical intensity and beam profile

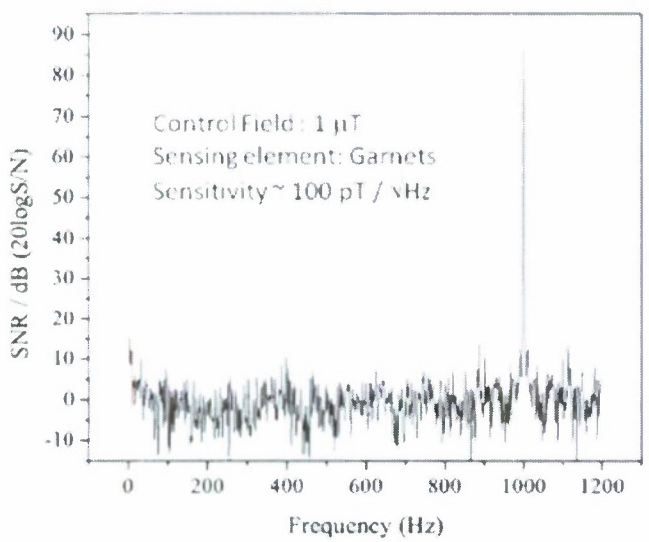

Figure 21. Typical data obtained from MO measurements system, in this case using ganet as a sample.

on the detectors even in the presence of mechanical vibrations. The total loss through the sample was estimated to be 4.5 dB which included loss from coupling and additional loss due to beam spreading. To estimate the minimum detectable magnetic field, a control magnetic field of 1 μT at 400 Hz was applied using an air-core solenoid (field measured using a hall-probe ac gauss meter) and the resulting signal and noise amplitudes were measured using the SR830 in a 0.26 Hz noise bandwidth. We measured a signal-to-noise ratio of 75dB (see Figure 21) from which we estimate a minimum detectable (noise-equivalent) field of 100 to 300 pT/√Hz.

5. Publications / Patent disclosures

Publications (published and communicated in 2008) and patent disclosures resulting from the work described above are listed.

i) Edith Botek, Benoît Champagne, Palash Gangopadhyay, André Persoons, and Thierry Verbiest, *Computing Letters,* **3**, 193 (2007).

ii) Palash Gangopadhyay, Ramakrishna Voorakaranam, Alejandra Lopez-Santiago, Stijn Foerier, Jayan Thomas, Robert A. Norwood, Andre Persoons, and Nasser Peyghambarian, *J. Phys. C.,* **C112**, 8032 (2008).

iii) Palash Gangopadhyay, Alejandra Lopez-Santiago and André Persoons, *Polymer Preprints*, **49**, 976 (2008).

iv) Palash Gangopadhyay, R. Voorakaranam, I. E. Araci, A. Lopez-Santiago, R. A. Norwood, V. J. Fratello, G. A. Oliver, R. R. Abbott, G. W. Berkstresser and N. Peyghambarian "*A sub-nanotesla magnetic field sensor using in-plane propagation of light in a negative-anisotropy garnet film"* manuscript submitted to CLEO 2009.

v) J. Thomas, Palash Gangopadhyay, and N. Peyghambarian "*NIMP: A new nanoimprinting technique for nanophotonic device fabrication*" manuscript submitted to NSTI Nanotech 2009.

vi) A. Lopez-Santiago, Palash Gangopadhyay, J. Thomas, R. A. Norwood, A. Persoons, and N. Peyghambarian, *"Faraday rotation in magnetite - polymethylmethacrylate core - shell nanocomposites with high optical quality"* Manuscript under preparation.

vii) J. Thomas, Palash Gangopadhyay, R. A. Norwood and N. Peyghambarian "*A new nanoimprinting technique for large area nanophotonic device fabrication*" manuscript under preparation.

viii) Palash Gangopadhyay, Guy Koeckelberghs, Alejandra Lopez-Santiago, Robert A. Norwood, Andre Persoons, Nasser Peyghambarian, "Low Temperature Magnetic Ordering in Regioregular Poly(3-dodecyl)thiophene Nano Doughnuts" Manuscript to be submitted.

ix) *Provisional US Patent application submitted on* "Magnetic Room Temperature Ionic Liquids as MO Materials", Palash Gangopadhyay and Robert A. Norwood.

Provisional US Patent application submitted on "Self assembled magnetic nanoparticle polymer composites with enhanced magneto-optic properties" Palash Gangopadhyay, A. Lopez-Santiago, J. Thomas and R. A. Norwood.

6. Interactions / Transitions

a) Participation/presentations at meetings, conferences, seminars etc.

i) *Poster and invited Presentation at International Conference on Organic Photonics and Electronics 2008,* ICOPE 08, Sata Fe, New Mexico, May 18 - 23, 2008.

ii) *Invited Presentation at* OSA conference on Organic Thin Films, Philadelphia, August 2008.

b) Consultative and advisory functions

References

1. Barr, E. S. "Men and Milestones in Optics. V. Michael Faraday," *Appl. Opt.* **1967**, *6*, 631.
2. Van Baak, D. A. *Am. J. Phys.*, **1996**, *64*, 724.
3. Winter, S.; Mok, C.; Kumarakrishnan, A. *Can. J. Phys.*, **2006**, *84*, 845.
4. Hafez, J. M.; Gao, J.; Eden, J. G. *Appl. Phys. Lett.*, **2007**, *90*, 132502, *and references there in.*
5. Affolderbach, C.; Stähler, M.; Knappe, S.; Wynands, R. *Appl. Phys. B.*, **2002**, *75*, 605.
6. Alfano, R. R.; Baird, D. H. *J. Appl. Phys.*, **1968**, *39*, 2931.
7. Chen, D. "Data Tabulations" CRC Handbook of Laser Science and Technology, Vol IV, Optical materials, Part 2: Properties, Weber M. J., ed., CRC Press, Cleveland, OH, **1986**.
8. (a) Gangopadhyay, P.; Foerier, S.; Koeckelberghs, G.; Vangheluwe, M.; Persoons, A.; Verbiest, T. *SPIE Proc., Linear and Nonlinear Optics of Organic Materials VI*, **2006**, *63301*, 63310Z1. (b) Koeckelberghs G.; Vangheluwe, M.; Persoons, A.; Verbiest, T *Macromol Rapid Comm.*, **2006**, *27*, 1920.
9. Rochfort, K. B.; Espejo, R. J.; Rose, A. H.; Dyer, S. D. *Optical Fiber Sensors*, **2000**, 332.
10. Zvezdin, A. K.; Kotov, V. A. *Modern Magnetooptics and Magnetooptical Materials*, Institute of Physics Publishing, **1997**, ISBN 0 7503 0362 X.
11. Sugano, S. ; Kojima, N. Editors, *Magneto-Optics*, Springer, **1999**, ISBN 3 540 65961 7..
12. Kominis, I. K.; Kornack, T. W.; Allred, J. C.; Romalis, M. V. *Nature*, **2003**, *422*, 596.
13. (a) Jain, A.; Kumar, J.; Zhou, F.; Li, L.; Tripathy, S. *Am. J. Phys.*, **1999**, *67*, 714. (b) Turvey, K. *Rev. Sci. Instrm.*, **1993**, *64*, 1561.
14. Pedrotti, F. L.; Bandettini, P. *Am. J. Phys.*, **1990**, *58*, 542.
15. Dodge, J. S.; Klein, L.; Fejer, M. M.; Kapitulnik, A. *J. Appl. Phys.*, **1996**, *79*, 6186, *and references there in.*
16. Xia, J.; Beyersdorf, P. T.; Fejer, M. M.; Kapitulnik, A. *Appl. Phys. Lett.*, **2006**, *89*, 062508.
17. Hwang, J.; Fejer, M. M.; Moerner, W. E. *Proceedings of SPIE*, **2003**, *4962*, 110.
18. The best case noise floor is constrained by the fundamental limit of shot noise and the shot noise limited noise floor of a photocurrent, i can be described as $i_n^{SN\,limited} = \sqrt{2ei\Delta f}$, where e is the electron charge and Δf is the detection bandwidth. See "Ultrasensitive laser measurements without tears," by P. C. D. Hobbs, *Appl. Opt.* **36** (4), 903 – 920, **1997** for details.
19. Beyersdorf, P. T.; Fejer, M. M.; Byer, R. L. *J. Opt. Soc. Am. B.*, **1999**, *16*, 1354.
20. http://www.st.northropgrumman.com/synoptics/SiteFiles/docs/PDFs/tgg_verdet_constant.pdf
21. Botek, E.; Champagne, B.; Verbiest, T.; Gangopadhyay, P.; Persoons, A. *Chem Phys Chem*, **2006**, *7*, 1654.
22. (a) Chen, T. A.; Wu, X.; Rieke, R. D. *J. Am. Chem. Soc.*, **1995**, *117*, 233. (b) Österbacka, R.; An, C. P.; Jiang, X. M.; Verdeny, Z. V. *Science*, **2000**, *287*, 839. (c) Kim, Y.; Cook, S.; Tuladhar, S. M.; Choulis, S. A.; Nelson, J.; Durrant, J. R.; Bradley, D. D. C.; Giles, M.; McCulloch, I.; Ha, C. S.; Ree, M. *Nat. Materials*, **2006**, *5*, 197.
23. Brown, P. J.; Thomas, D. S.; Köhler, A.; Wilson, J. S.; Kim, J. S.; Ramsdale, C. M.; Sirringhaus, H.; Friend, R. H. *Phys. Rev.*, **2003**, *B67*, 064203.

[24]. Sirringhaus, H.; Brown, P. J.; Friend, R. H.; Nielsen, M. M.; Bechgaard, K.; Langeveld-Voss, B. M. W.; Spiering, A. J. H.; Janssen, R. A. J.; Meijer, A. E.; Herwig, P.; de Leeuw, D. M. *Nature*, **1999**, *401*, 685.

[25]. Zhang, R.; Li, B.; Iovu, M. C.; Malika, J.; de Sauve, G.; Cooper, J.; Jia, S.; Tristram-Nagle, S.; Smilgies, D. M.; Lambeth, D. N.; McCullough, R. D.; Kowalewski, T. *J. Am. Chem. Soc.*, **2006**, *128*, 3480.

[26]. Kline, R. J.; McGehee, M. D.; Kadnikova, E. N.; Liu, J.; Frechet, J. M. J. *Adv. Mater.*, **2003**, *15*, 1519.

[27]. Chang, J.; Sun, B.; McCullough, I.; Sirringhaus, H. *Chem. Mater.*, **2004**, *16*, 4772.

[28]. Wu, Y.; Liu, P.; Gardner, S.; Ong, B. S. *Chem. Mater.* **2005,** *17*, 221.

[29]. Yamamoto, T.; Komarudin, D.; Arai, M.; Lee, B.-L.; Suganuma, H.; Asakawa, N.; Inoue, Y.; Kubota, K.; Sasaki, S.; Fukuda, T.; Matsuda, H. *J. Am. Chem. Soc.* **1998**, *120*, 2047.

[30]. Zvara, M. *Phys. Stat. Sol.*, **1969**, *36*, 785.

[31]. Dennis, R. B.; Smith, S. D.; Summers, C. J. *Proc. Roy. Soc. Lond. A*, **1971**, *321*, 303.

[32]. Awschalom, D. D.; Halbout, J. M.; von Molner, S.; Siegrist, T.; Holtzberg, F. *Phys. Rev. Lett.*, **1985**, *55*, 1128.

[33]. Baer, W. S. *Phys. Rev.*, **1967**, *154*, 786.

[34]. Skotheim, T. A.; Reynolds, J. R., Editors, *Handbook of Conducting Polymers*, 3rd. Edition, CRC Press, New York, **2007**, ISBN # 1-4200-4360-9.

[35]. Tanase, C.; Meijer, E. J.; Blom, P. W. M.; de Leeuw, D. M., *Phys. Rev. Lett.*, **2003**, *91*, 216601.

[36]. Wang, Z.; Mazumdar, S.; Shukla, A. arXiv:0712.1065v1 [cond-mat.str-el]

[37]. Arita, R.; Kuroki, K.; Aoki, H. *Phys. Rev. B*, **2000**, *61*, 3207.

[38]. Gangopadhyay, P. *et. al.*; *Unpublished results*.

[39]. Mermer, Ö.; Veeraraghavan, G.; Francis, T. L.; Sheng, Y.; Nguyen, D. T.; Wohlgenannt, M.; Köhler, A.; Al-Suti, M. K.; Khan, M. S. *Phys. Rev. B*, **2005**, *72*, 205202.

[40]. a) J. S. Miller, M. Drillon, *Magnetism: Molecules to Materials, Models and Experiments* Wiley-VCH, New York, **2001**; c) S. J. Blundell, F. L. Pratt, *J. Phys.: Condens. Matter* **2004**, *16*, R771; d) J. S. Miller, *Pramana – J. Phys.* **2006**, *67*, 1.

[41]. a) A. K. Zvezdin, V. A. Kotov, *Modern Magnetooptics and Magnetooptical Materials*, Institute of Physics Publishing, Philadelphia, **1997**; b) J. S. Miller, *Adv. Mater.*, **2002**, *14*, 1105.

[42]. a) K. Itoh, M. Kinoshita, *Molecular Magnetism*, Gordon & Breach, Kodansha, Tokyo, **2000**; b) A. Rajca, *Chem. Eur. J.*, **2002**, *8*, 4835.

[43]. a) F. M. Romero, R. Ziessel, M. Bonnet, Y. Pontillon, E. Ressouche, J. Schweizer, B. Delley, A. Grand, C. Paulsen *et. al. J. Am. Chem. Soc.*, **2000**, *122*, 1298; b) D. Maspoch, N. Domingo, D. Ruiz-Molina, K. Wurst, G. Vaughan, J. Tejada, C. Rovira, and J. Veciana. *Angew. Chem. Int. Ed.*, **2004**, 43, 1828; c) Y. Z. Zheng, M. Tong, W. Xue, W. Zhang, X. Chen, F. Grandjean, G. J. Long, *Angew. Chem. Int. Ed.*, **2007**, *46*, 6076.

[44]. a) H. Fukutome, A. Takahashi, M. Ozaki, *Chem. Phys. Lett.*, **1987**, *133*, 34; b) M. M. Murray, P. Kaszynski, D. A. Kaisaki, W. Chang, D. A. Dougherty, *J. Am. Chem. Soc.*, **1994**, *116*, 8152; c) H. Nishide, T. Kaneko, T. Nii, K. Katoh, E. Tsuchida, K. Yamaguchi, *J. Am. Chem. Soc.*, **1995**, *117*, 548; d) M. Kinoshita, *Proc. Jpn. Acad.*, **2004**, *B80*, 41; e) H. Iwamura, *Proc. Jpn. Acad.*, **2005**, *B81*, 233, and references therein.

[45]. a) R. Arita, K. Kuroki, H. Aoki, *Phys. Rev. B*, **2000**, *61*, 3207; b) A. P. Monkman, H. D. Burrows, L. J. Hartwell, L.E. Horsburgh, I. Hamblett, S. Navaratnam, *Phys. Rev. Lett.*, **2001**, *86*, 1358; c) R. Arita, Y. Suwa, K. Kuroki, H. Aoki, *Phys. Rev. Lett.*, **2002**, *88*, 127202; d) A. Tanaka, H. Tasaki, *Phys. Rev. Lett.*, **2007**, *98*, 116402.

[46]. a) A. Rajca, J. Wongsriratanakul, S. Rajca, R. Cerny, *Angew. Chem. Int. Ed.*, **1998**, *37*, 1229; b) A. Rajca, J. Wongsriratanakul, S. Rajca, *J. Am. Chem. Soc.*, **2004**, *126*, 6608; c) A. Rajca, M. Miyaska, Chapter 15 in *Functional Organic Materials – Synthesis and Strategies*, (Eds.: T. J. J. Mueller, U. H. F. Bunz) Wiley-VCH, New York, **2007**; d) A. Rajca, M. Takahashi, M. Pink, G. Spagnol, S. Rajca, *J. Am. Chem. Soc.*, **2007**, *129*, 10159.

[47]. A. Rajca, J. Wongsriratanakul, S. Rajca, *Science*, **2001**, *294*, 1503.

[48]. a) M. Miyasaka, T. Yamazaki, E. Tsuchida, H. Mishide, *Macromolecules*, **2000**, *33*, 8211; b) N. Blouin, M. Leclerc, B. Vercelli, S. Zecchin, G. Zotti, *Macromol. Chem. Phys.*, **2006**, *207*, 175.

[49]. a) H. Sirringhaus, P. J. Brown, R. H. Friend, M. M. Neilsen, K. Bechgaard, B. M. W. Langeveld, A. J. H. Spiering, R. A. J. Janssen, E. W. Meijer, P. Herwig, D. M. de Leeuw, *Nature*, **1999**, *401*, 685. b) R. Österbacka, C. P. An, X. M. Jiang, Z. V. Vardeny, *Science*, **2000**, *287*, 839; b) R. J. Kline, M. D. McGhee, M. F. Toney, *Nature Mat.*, **2006**, *5*, 222; c) Y. Kim, S. Cook, S. M. Tuladahar, S. A. Choulis, J. Nelson, J. R. Durrant, D. D. C. Bradley, M. Giles, I. McCulloch, C. S. Ha, M. Ree, *Nature Mat.*, **2006**, *5*, 197; d) G. Koeckelberghs, M. Vangheluwe, K. Van Doorsselaere, A. Persoons, T. Verbiest, *Macromol. Rapid Comm.*, **2006**, *27*, 1920.

[50]. P. J. Brown, D. S. Thomas, A. Köhlar, J. S. Wilson, J. S. Kim, C. M. Ramsdale, H. Sirringhaus, R. H. Friend, *Phys. Rev. B.*, **2003**, *63*, 064203.

[51]. a) S. A. Chen, J. M. Ni, *Macromolecules*, **1992**, *25*, 6081; b) N. T. Binh, L. Q. Minh, H. Bässler, *Synth. Met.*, **1993**, *58*, 39.

[52]. a) H. Sakaguchi, H. Matsumura, H. Gong, *Nature Mat.*, **2004**, *3*, 551; b) R. J. Kline, M. D. McGhee, *J. MacroMol. Sci.*, **2006**, *C46*, 27; c) J. Chang, J. Clark, N. Zhao, H. Sirringhaus, D. W. Breiby, J. W. Andreasen, M. M. Neilsen, M. Giles, M. Heeney, I. McCulloch, *Phys. Rev. B*, **2006**, *74*, 115318.

[53]. Magnetic measurements were carried out using DC/AC (SQUID) MPMSS susceptometer.

[54]. a) T. Moriya, *Spin Fluctuations in Itinerant Electron Magnetism*, Springer-Verlag, Berlin, **1985**; b) H. Tasaki, *Phys. Rev. Lett.*, **1992**, *69*, 1608.

[55]. a) A. E. Berkowitz, E. Kneller, *Magnetism and Mettallurgy*, Academic Press, New York, **1969**, p. 393; b) R. L. Carlin, *Magnetochemistry*, Springer-Verlag, New York, **1986**.

[56]. The diameter was calculated using a spherical shape factor and the low field magnetization data; a blocking temperature of 5 K was used. For details see ref. 13.

[57]. a) R. Sessoli, D. Gatteschi, A. Caneschi, M. A. Novak, *Nature*, **1993**, *365*, 141; b) J. A. Mydosh, *Spin Glasses, an Experimental Introduction*, Taylor and Francis, London, **1993.**

[58]. T. Jonsson, P. Nordblad, P. Svedlindh, *Phys. Rev. B*, **1998**, *57*, 497.

[59]. S. –H. Lee, C. Broholm, G. Aeppli, A. P. Ramirez, T. G. Perring, C. J. Charlie, M. Adams, T. J. L. Jones, B. Hessen, *Europhysics Lett.*, **1996**, *35*, 127.

[60]. 1 spin in ~100000 chains is relatively small compared to earlier reported values of 1 spin in ~1200 chains, i.e., 5 x 10^{16} spins/g, making **1** virtually defect less; see for reference, G. Cik, F. Sersen, L. Dlhan, L. Szabo, J. Bartus, *Synth. Met.*, **1995**, *75*, 43.

[61]. B. B. Van Aken, J. P. Rivera, H. Schmid, M. Fiebig, *Nature*, **2007**, *449*, 702.

[62]. W. R. Wadt, W. R. Moomaw, *Molecular Physics*, **1973**, *25*, 1291.

[63]. Ö. Mermer, G. Veeraraghavan, T. L. Francis, Y. Sheng, D. T. Nguyen, M. Wohlgenannt, A. Köhler, M. K. Al-Suti, M. S. Khan, *Phys. Rev. B*, **2005**, *72*, 205202.

[64]. J. Lenz and A.S. Edelstein, *IEEE Sensors Journal*,**2006,** *6*. 3.

[65]. M.N. Deeter, A.H. Rose and G.W. Day, *Proc. SPIE*, **1990**, *1367*, 243.

[66]. V. J. Fratello, I. Mnushkina, S. J. Licht and R. R. Abbott, *Mater. Res. Soc. Symp. Proc.* 2005, *834*, J6.2.2.